Dynamics of Thin Polymer Films: Recent Insights from Incoherent Neutron Scattering

CHRISTOPHER L. SOLES, JACK F. DOUGLAS, WEN-LI WU

Polymers Division, National Institute of Standards and Technology, Gaithersburg, Maryland 20899-8541

Received 30 October 2003; revised 18 February 2004; accepted 20 February 2004
DOI: 10.1002/polb.20172
Published online in Wiley InterScience (www.interscience.wiley.com).

ABSTRACT: Incoherent neutron scattering is presented as a powerful tool for interpreting changes in molecular dynamics as a function of film thickness for a range of polymers. Motions on approximately nanosecond and faster timescales are quantified in terms of a mean-square atomic displacement ($\langle u^2 \rangle$) from the Debye–Waller factor. Thin-film confinement generally leads to a reduction of $\langle u^2 \rangle$ in comparison with the bulk material, and this effect becomes especially pronounced when the film thickness approaches the unperturbed dimensions of the macromolecule. Generally, there is a suppression (never an enhancement) of $\langle u^2 \rangle$ at temperatures T above the bulk calorimetric glass-transition temperature (T_g). Below T_g, the reduction in the magnitude of $\langle u^2 \rangle$ depends on the polymer and the length scales being probed. Polymers with extensive segmental or local mobility in the glass are particularly susceptible to reductions of $\langle u^2 \rangle$ with confinement, especially at the $\mathbf{Q}$ vectors probing these longer length scales, whereas materials lacking these sub-T_g motions are relatively insensitive. Moreover, a reduced $\langle u^2 \rangle$ value correlates with reduced mobility at long time and spatial scales, as measured by diffusion in these thin polymer films. Finally, this reduced thin-film mobility is not reliably predicted by thermodynamic assessments of an apparent T_g, as measured by discontinuities or kinks in the T dependence of the thermal expansion, specific volume, index of refraction, specific heat, and so forth. These measurements illustrate that $\langle u^2 \rangle$ is a powerful and predictive tool for understanding dynamic changes in thin polymer films. © 2004 Wiley Periodicals, Inc.* J Polym Sci Part B: Polym Phys 42: 3218–3234, 2004

Keywords: diffusion; neutron scattering; thin films

INTRODUCTION

Recently, the scientific literature has been flooded with experimental studies addressing the effects of film thickness on the glass-transition temperature (T_g; see two recent reviews[1,2] for a representative list of references). This activity is motivated by the widespread use of polymer thin films in numerous emerging technologies (coatings and barriers, adhesives, lithography, sensors, nanodevices, etc.) and by the potential insight that these measurements bring into the mysterious process of glass formation. Regardless of our poor understanding of bulk glass formation, there is an established phenomenology linking thermodynamic measurements, such as thermal expansion and specific heat, to the dramatic changes in bulk transport properties [viscosity (η) and diffusion] that embody the liquid–glass transition. Normally, T_g is operationally defined by a kink in these thermodynamic properties as a function of

Correspondence to: C. L. Soles (E-mail: csoles@nist.gov)

Journal of Polymer Science: Part B: Polymer Physics, Vol. 42, 3218–3234 (2004)

temperature T, with the understanding that the kink position (T_g) is influenced by the rate of cooling of the fluid into the glassy state.

Extensions of this operational definition to thin films or confined geometries naturally lead to basic questions regarding the nature of the glass transition. Specifically, it is not clear *a priori* whether thermodynamic estimates of the glass transition based on bulk materials are predictive of mobility changes in thin films, or even if a unique thermodynamic transition exists. Indeed, the measurements described herein show that conventionally defined T_g estimates are property specific and that apparent T_g shifts with the film thickness can even be anticorrelated with changes in the molecular mobility under confinement. The whole question of a T_g determination in thin films may then seem somewhat ill posed with respect to the prediction of mobility changes upon confinement. Because of this unsatisfactory situation, it is now critical to develop reliable metrologies to quantify mobility changes in thin polymer films.

DYNAMICS FROM NEUTRON SCATTERING

This article builds upon a recent series of incoherent neutron scattering measurements[3–5] that quantify the amplitude of the local, high-frequency atomic motions in a range of thin polymer films. We contend that these measurements provide a more useful assessment of the dynamics in films than could be inferred from the aforementioned operational definition of a T_g based on thermodynamic parameters. The inelastic neutron scattering spectrum contains detailed information about the timescale and geometry of all the atomic motions. These motions are often described by the one-phonon approximation:

$$S_{inc}(\mathbf{Q},\omega) = \frac{3N\hbar}{2M} e^{-2W}\mathbf{Q}^2 \frac{n(\omega)+1}{\omega} g(\omega) \quad (1)$$

where $S_{inc}(\mathbf{Q},\omega)$ is proportional to the number of neutrons scattered at a wavevector $\mathbf{Q}$ with a frequency ω, $g(\omega)$ is the density of states, $n(\omega) + 1$ is the Bose population factor, and e^{-2W} is the Debye–Waller factor. In this expression, W is equal to $(1/6)\mathbf{Q}^2\langle u^2\rangle$, where $\langle u^2\rangle$ is the mean-square atomic displacement. It is $S_{inc}(\mathbf{Q},\omega)$ that contains the detailed information about the timescale (ω) and geometry ($\mathbf{Q}$) of the atomic motions. However, $S_{inc}(\mathbf{Q},\omega)$ at $\omega \neq 0$ is typically several orders of magnitude smaller than the elastic scattering at $\omega = 0$, especially in the glassy state. In thin polymer films, in which the sample mass is limited, we find that the inelastic scattering becomes comparable to the experimental noise and difficult to quantify. However, the changes in the stronger elastic scattering intensity $I_{elastic}$ also contain information, albeit less detailed, about the sample dynamics. The total scattering must be conserved, and this means that an increase in the inelastic scattering (due to molecular mobility) necessitates a reduction of the elastic scattering. For elastic incoherent scattering, the $\mathbf{Q}$ dependence of this elastic scattering is often approximated with the Debye–Waller factor:

$$I_{elastic}(\mathbf{Q}) \propto \exp(-\tfrac{1}{3}\mathbf{Q}^2\langle u^2\rangle) \quad (2)$$

Within this model, based on a harmonic oscillator, the slope of $\ln[I_{elastic}(\mathbf{Q})]$ versus $\mathbf{Q}^2$ is equal to $\langle u^2\rangle/3$. Although most atomic motions in soft condensed matter are admittedly anharmonic, this approximation has been useful for characterizing the dynamics in both synthetic[6–10] and biological[11–15] macromolecules. In this study and our previous studies,[3–5] we have extended this utility to include confinement effects in thin polymer films.

EXPERIMENTAL

Materials

Thin films of polycarbonate (PC), poly(methyl methacrylate) (PMMA), poly(vinyl chloride) (PVC), and poly(*tert*-butoxycarboxystyrene) (PBOCSt) were spin-cast from solutions onto clean Si wafers. The solutions were prepared through the dissolution of PC (GE Lexan ML-4235;[16] $M_{r,w}$[†] = 36.3 kg/mol), PMMA (Polymer Source; $M_{r,w}$ = 1730 kg/mol), PVC (Aldrich; $M_{r,w}$ = 233 kg/mol), and PBOCSt (synthesized as described elsewhere;[17,18] $M_{r,n}$ = 8 kg/mol) at various mass fractions into cyclohexanone, toluene, cyclohexanone, and pro-

[†]According to ISO 31-8, the term "molecular weight" has been replaced by "relative molecular mass," symbol M_r. Thus, if this nomenclature and notation were to be followed in this publication, one would write $M_{r,w}$ instead of the historically conventional M_w for the mass average molecular weight, with similar changes for M_n, M_z, and M_v, and it would be called the "mass average relative molecular mass."

pylene glycol methyl ether acetate, respectively. These solutions were filtered through 0.45-μm Teflon filters. Thin ⟨100⟩ Si wafers (Silicon, Inc.; 13–17 mil thick and 75 mm in diameter) were O_2-plasma-cleaned to remove residual organic contaminants and were treated with HF acid to remove the native silicon oxide surface. A controlled oxide layer was then regrown in a UV ozone chamber to a thickness of 10–20 Å. The polymer solutions were immediately spin-cast at 209 rad/s (2000 rpm) onto the clean, hydrophilic wafers to create thin films. With some of the PMMA films, additional steps were taken to render the Si substrate hydrophobic. After the UV ozone exposure, hexamethyldisilizane was added dropwise onto the wafers, and they were baked on a hotplate at 200 °C for 2 min. This replaced the surface Si—OH groups of the silicon oxide with Si—CH_3 groups, leaving a visibly hydrophobic surface. Immediately after the spin coating, the films (expect for the PBOCSt ones) were heated to T_g + 20 °C for at least 6 h under a vacuum better than 10^{-4} Pa to remove the residual solvent. The residual solvent was removed from the PBOCSt films with a similar vacuum with a 12-h postapplication bake at 120 °C. The final film thickness in each case was measured at room temperature with X-ray reflectivity.

Incoherent Neutron Scattering

The incoherent neutron scattering experiments were performed at the National Institute of Standards and Technology Center for Neutron Research on the high-flux backscattering spectrometer (HFBS)[19] located on the NG2 beam line. This spectrometer uses cold neutrons with a wavelength of 6.271 Å and accesses a **Q** range of 0.25–1.75 $Å^{-1}$. This is important because the Bragg diffraction peaks for the Si substrates or Al sample cell are beyond the **Q** range of the spectrometer and are, therefore, not visible. The neutron absorption coefficients for both Si and Al are also low, and this ensures that the hydrogenous polymer dominates the scattering. Likewise, the vibrational amplitudes in the crystalline Si are much smaller than those of any soft polymeric material, and this further ensures that the dynamics of Si are negligible. The 0.8-μeV full-width-at-half-maximum energy resolution of the spectrometer dictates that only those motions 200 MHz or faster will contribute to the reduction in the elastic scattering; slower motions appear as elastic scattering.

The HFBS sample cells were thin-walled Al cans approximately 25 mm in diameter and 50 mm high. To maximize the scattering signal from our thin polymer films, 13–15 of the coated wafers were cleaved into 50-mm strips (of various widths) and placed inside the sample cells. This resulted in approximately 0.5–10 mg of the polymer per cell, in contrast to the 52–58 g of Si. Each sample cell was then mounted on the HFBS spectrometer, placed under a vacuum, and cooled to 30–50 K. Data were collected as the samples were heated at a rate of 0.1–0.5 K/min up to 525 K. The scattered intensities in each detector (each **Q**; there were 16 detectors) were binned into temperature intervals of 1–3 K to increase the counting statistic. Slower heating rates were required for the thinner films to obtain reasonable counting statistics. The measurement times for the thinnest films were approximately 3–4 days.

RESULTS

Figure 1 displays the T dependence of the elastic scattering intensity, summed over the entire **Q** range of the spectrometer, for oxide-supported PC, PMMA, and PVC films. The intensities have been normalized to unity at the lowest temperature for a comparison of films of different thicknesses. As mentioned previously, an intensity decrease corresponds to an increase in the amplitude of the atomic motion, which we interpret as an increase in mobility. The HFBS spectrometer has sufficient sensitivity to probe the dynamics in films as thin as 75 Å, as evidenced in Figure 1(A,B) by the noticeable difference between the thinnest films and the blank Si. We acknowledge that the decrease in the intensity for the blank wafers is more significant than that anticipated for pure Si. This is probably due to residual surface contamination on the sample can, heat shields, walls of the spectrometer, and so forth that cannot be removed. Nevertheless, Figure 1 indicates that the extent of mobility is reduced as the film thickness decreases. The normalized thermal reduction of the elastic intensity becomes less significant in increasingly thin films. By analyzing the **Q** dependence of these changes, we can estimate $\langle u^2 \rangle$ with eq 2.

The **Q** dependence of the elastic scattering as a function of T for the thinnest PC and PMMA films is shown in Figure 2. The lowest T data set, which is generally between 30 and 50 K, has been used to normalize all the higher T elastic intensities.

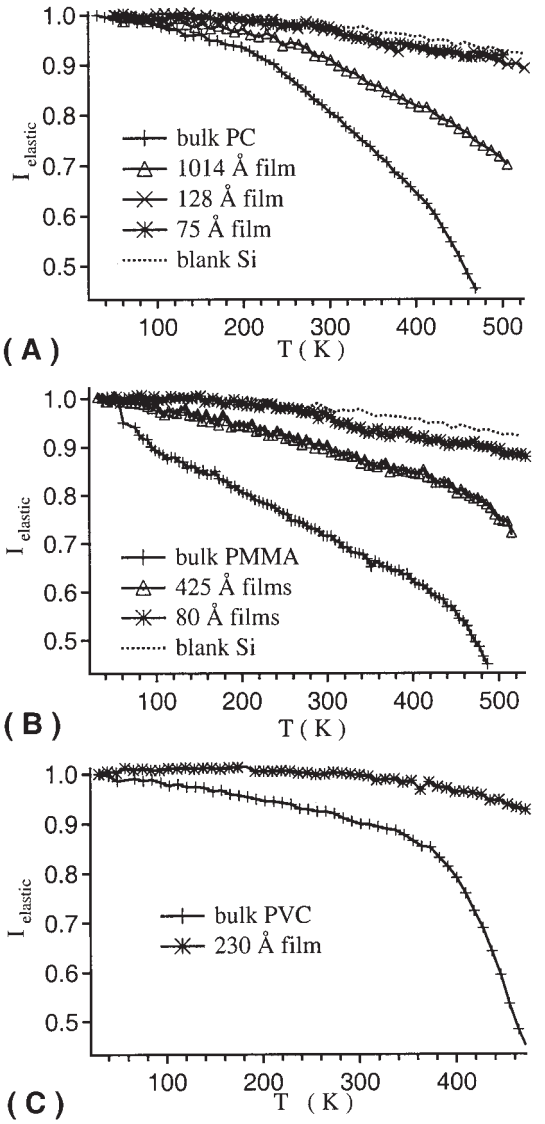

Figure 1. $I_{elastic}$, summed over all available detectors, as a function of T for (A) PC, (B) PMMA, and (C) PVC films. For each sample, $I_{elastic}$ has been normalized by the lowest T value. The decrease in $I_{elastic}$ upon heating directly reflects the thermal motion in the polymer film. As the film thickness decreases, there is a strong reduction of this thermal mobility. The standard uncertainties of the $I_{elastic}$ values are less than or comparable to the size of the data markers.

According to the Debye–Waller approximation, a normalized ln $I_{elastic}$–$\mathbf{Q}^2$ plot (where $I_{elastic}$ is the elastic neutron scattering intensity) yields a straight line with the slope proportional to $\langle u^2 \rangle/3$. The normalization allows us to directly compare $\langle u^2 \rangle$ values for films of different thicknesses. The mass of the scattering sample in the beam enters eq 1 through the term $3Nh/2M$, which lies outside the exponent of the Debye–Waller factor. By taking the ratio, we find that the sample mass (thickness) drops out of the $\langle u^2 \rangle$ calculation. For the 75-Å PC film, the linear approximation is reasonable for the $\mathbf{Q}^2$ range below 1.0 Å^{-2}. However, the inset reveals deviations from linearity above $\mathbf{Q}^2$ = 1.0 Å^{-2}, with an apparent maximum near $\mathbf{Q}^2$ = 1.5^{-2} Å^{-2} in both the bulk and thin-film data. Previously, we noted that this maximum nomi-

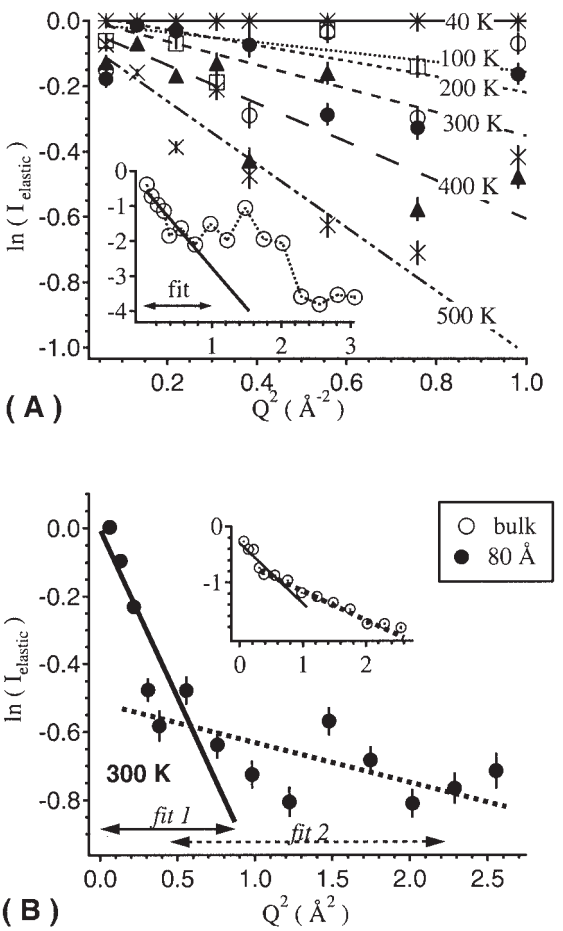

Figure 2. Typical ln $I_{elastic}$–$\mathbf{Q}^2$ plots used to estimate $\langle u^2 \rangle$. In this representation, $\langle u^2 \rangle$ is proportional to the slope of a linear fit through the data. (a) Isothermal fits for the 75-Å PC film at $\mathbf{Q}^2 < 1.0$ Å^{-2}. As the temperature increases, the larger slope corresponds to an increase in $\langle u^2 \rangle$. The inset displays an analogous plot for bulk PC at 300 K. There is a peak in the bulk data near $\mathbf{Q}^2$ = 1.5 Å^{-2} (possible origins of this peak, which is also present in the thin-film data, are discussed in the text). (b) Same type of data for bulk and 80-Å PMMA films. For PMMA, the bulk data reveal two quasilinear regimes (the implications of using the two different fitting regimes are discussed later). The error bars indicate the standard uncertainty of the scattered intensity.

nally coincides with the peak in the static structure factor, which is commonly called the amorphous halo ($\mathbf{Q}^2 = 1.6$ Å^{-2}).[12] From this, we surmised that the strong deviation from linearity in PC indicates coherent neutron scattering, especially at high temperatures, at which the deviation is most pronounced.

In addition to PC, Figure 2 shows ln I_{elastic}–$\mathbf{Q}^2$ curves for PMMA at 300 K for both 80-Å films and the bulk (inset). As with PC, the region below $\mathbf{Q}^2 = 1.0$ Å^{-2} is reasonably linear in both the thin film and bulk. In the region beyond $\mathbf{Q}^2 = 1.0$ Å^{-2}, the PMMA dependence is now linear, without the maximum that is evident for PC. Although it is not explicitly shown here, the $\mathbf{Q}$ dependence of the PVC elastic intensities qualitatively resembles that of PMMA. At this time, we do not completely understand why PC differs from PMMA and PVC in the high-$\mathbf{Q}$ region. Regardless of their differences at high-$\mathbf{Q}$, PC, PMMA, and PVC show similar trends in the low-$\mathbf{Q}$ region, and there is always a break in the slope near $\mathbf{Q}^2 = 1.0$ Å^{-2}. This reflects the fact that the motions are considerably more complicated than those predicted by the harmonic Debye–Waller model. Nonlinear dependencies of ln I_{inc} on $\mathbf{Q}^2$ have been reported for a number of polymer[7] and biological[11,13,14,20] systems, and there have been attempts to calculate $\langle u^2 \rangle$ with more complicated models. These models generally embody both a Gaussian (harmonic) component and a non-Gaussian component, the latter being thermally activated and dominant at low $\mathbf{Q}$.[7,11,13,14,20] However, these models also increase the number of curve-fitting parameters, so it is not entirely clear if the added parameters increase our understanding of the motions. Furthermore, we must fit the data to very high $\mathbf{Q}$ values to reliably separate the local harmonic motions (high $\mathbf{Q}$) from the long-range anharmonic contributions (low $\mathbf{Q}$). The HFBS spectrometer is not designed to access these high-$\mathbf{Q}$ regions of phase space.

Given the $\mathbf{Q}$ range of our spectrometer and the nature of the thin-film data presented, we take a simplified approach and limit the $\langle u^2 \rangle$ analysis to the regime below $\mathbf{Q}^2 = 1.0$ Å^{-2}. This region appears consistent between different types of polymers and avoids peaklike features or upturns in the high-$\mathbf{Q}$ data. Of course, the $\langle u^2 \rangle$ values extracted from this harmonic approximation are not exact in light of the anharmonicity evidenced in Figure 2. It is well known that analyzing this low-$\mathbf{Q}$ data emphasizes some of the longer range motions, such as methyl rotations,[7] that are not completely within the framework of a harmonic oscillator. Nevertheless, the low-$\mathbf{Q}$ estimate of $\langle u^2 \rangle$ provides a reasonable and consistent framework for comparing thin-film confinement effects between the different polymers. We demonstrate the generality of this approach through the PMMA and PVC films; the absence of the strong high-$\mathbf{Q}$ peak allows us to fit two linear functions (one low-$\mathbf{Q}$ and one high-$\mathbf{Q}$) through the data, as illustrated in Figure 2. This allows us to compare the $\langle u^2 \rangle$ trends from the low-$\mathbf{Q}$ and high-$\mathbf{Q}$ regions. Although the absolute values of $\langle u^2 \rangle$ from the two regions differ, the trends with increasing confinement are similar.

The differences between the low-$\mathbf{Q}$ and high-$\mathbf{Q}$ estimates of $\langle u^2 \rangle$ are evident in the insets of Figures 3(B,C); the main graph of each figure reflects fits with the region $\mathbf{Q}^2 < 1.0$ Å^{-2}, whereas the inset emphasizes the $0.3 < \mathbf{Q}^2$ (Å^{-2}) < 2.3 data. Choosing to analyze the low-$\mathbf{Q}$ region leads to larger $\langle u^2 \rangle$ values. For example, at the calorimetric T_g of bulk PMMA (395 K), $\langle u^2 \rangle$ is 1.3 Å^2 for the low-$\mathbf{Q}$ data, whereas $\langle u^2 \rangle$ is 0.8 Å^2 for the higher $\mathbf{Q}$ fit; a similar observation holds true for PVC. This is reasonable as the low-$\mathbf{Q}$ data reflect longer range motions. What is more important is that the trend with decreasing film thickness is generally similar for the two regions: a reduction of $\langle u^2 \rangle$ with decreasing film thickness and, for PMMA, no differences between the hexamethyldisilazane (HMDS) and oxide surfaces. Although focusing on the low-$\mathbf{Q}$ region may emphasize longer range motions that potentially deviate from the harmonic Debye–Waller criteria at high temperatures, the general indication of how the dynamics respond to confinement is reasonable. This should be borne in mind when we consider the absolute magnitudes of $\langle u^2 \rangle$ values in this work. In the most of this article, the primary emphasis is $\langle u^2 \rangle$ extracted from the region $\mathbf{Q}^2 < 1.0$ Å^{-2}.

Figure 3 displays the low-$\mathbf{Q}$ estimates of $\langle u^2 \rangle$ as a function of the film thickness and temperature for PC, PMMA, and PVC films. Once again, the general trend is that decreasing film thickness leads to a suppression of $\langle u^2 \rangle$. In PVC, this suppression is primarily above the bulk calorimetric T_g of 358 K; deep in the glassy state, there is little change in $\langle u^2 \rangle$ with confinement. This is unlike the PC films (and, to a lesser extent, the PMMA films), which show large suppressions of $\langle u^2 \rangle$ far below the bulk calorimetric T_g. At first, this may seem inconsistent with Figure 1(C), which shows strong differences in the thermal evolution of the

scattering intensities between the bulk PVC and the 220-Å film. Although that these intensities are summed over the entire **Q** range of the spectrometer, the main portion of Figure 3(C) represents the low-**Q** data. The inset to Figure 3(C), focusing on the high-**Q** data, does reveal a strong difference between the bulk and 220-Å PVC films below T_g, and this is consistent with the reduced intensities in Figure 1(C). Likewise, if Figure 1(C) is repeated with just the high-**Q** detectors summed, there is noticeable difference between the bulk and thin-film data. This is an important distinction to make; the choice of the fit region affects the $\langle u^2 \rangle$ values, and it is important to understand this influence on the $\langle u^2 \rangle$ estimates. This is addressed further in the Discussion section.

It remains to be seen if the motions reflected in $\langle u^2 \rangle$ are isotropic or preferentially oriented either perpendicularly or parallel to the plane of the film. The fact that we primarily use the low-**Q** grouping of detectors can be used to test for such anisotropy. Because the films are stacked with their surfaces parallel, the sample holder can be rotated so that **Q** is either mostly parallel or perpendicular to the plane of the films. These two sample orientations emphasize $\langle u^2 \rangle$ in the plane of the film and normal to the substrate, respectively. Figure 4 demonstrates this on the 425-Å PMMA films supported on the oxide substrate. It appears that $\langle u^2 \rangle$ is relatively isotropic in the films; there are no differences between **Q**-parallel and **Q**-perpendicular orientations within the sensitivity of the technique.

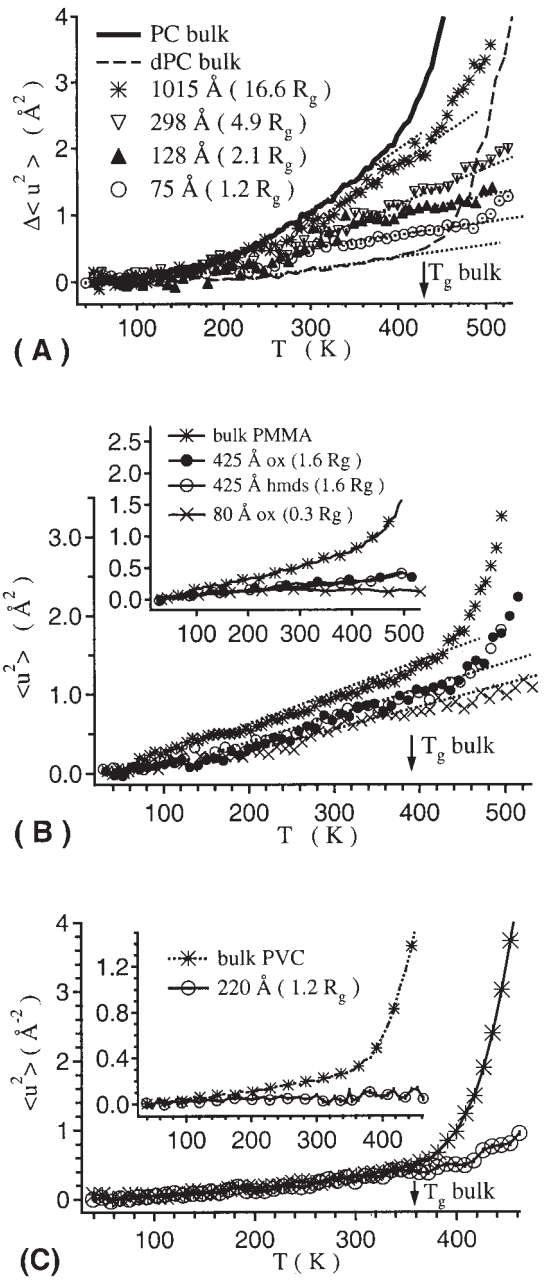

DISCUSSION

Effects of Thin-Film Confinement on $\langle u^2 \rangle$

As the thickness of a polymer film is continually reduced, eventually the state is reached in which the film thickness must distort the configuration of the macromolecules. Although the precise length scale at which this distortion occurs remains ambiguous, a high-molecular-mass poly-

Figure 3. Hydrogen-weighted $\langle u^2 \rangle$ values plotted as a function of temperature for (A) PC, (B) PMMA, and (C) PVC films. The data for the main graphs were obtained from linear fits at $\mathbf{Q}^2 < 1.0$ Å^{-2} (as demonstrated in Fig. 2). The legends indicate the film thickness in units of the unperturbed chain dimensions (i.e., R_g). There are also alternative data sets for the PMMA and PVC films in the insets (each axis has the same units as the main graph), illustrating the differences in $\langle u^2 \rangle$ that stem from the use of the high-**Q** linear fitting regimes shown in Figure 2 and the use of the low-**Q** regimes. Although the magnitudes of $\langle u^2 \rangle$ are strongly affected by the choice of the fitting regime, the general trends with the film thickness are qualitatively similar. The deuterated polycarbonate (dPC) curve demonstrates that $\langle u^2 \rangle$ is significantly reduced when the hydrogenous segmental motions in bulk PC are masked by the replacement of hydrogen with deuterium. The standard uncertainties of $\langle u^2 \rangle$ are typically comparable to the size of the data markers.

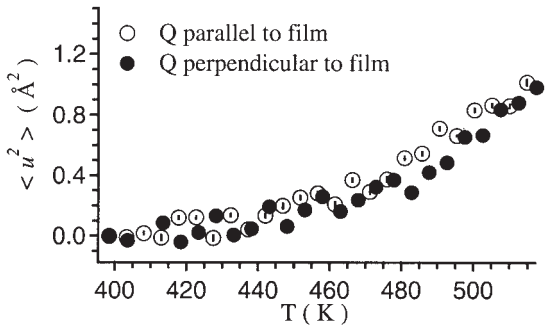

Figure 4. $\langle u^2 \rangle$ values for a 425-Å PMMA film oriented so that the scattering vectors of the analyzed low-**Q** detector bank are either parallel or perpendicular to the plane of the film, probing for in-plane and out-of-plane motions, respectively. Within the sensitivity of the spectrometer, $\langle u^2 \rangle$ is isotropic in the film. The standard uncertainties of $\langle u^2 \rangle$ are less than the size of the data markers.

mer would seemingly feel this distortion of confinement in thicker films than a low-molecular-mass analogue. In this respect, it is reasonable to normalize the film thickness (h) in terms of the approximate molecular size or the radius of gyration (R_g). The R_g estimates for PC, PMMA, and PVC used here under θ conditions are 61,[21] 262,[22] and 179 Å,[23] respectively. The legends in Figure 3 indicate h in multiples of the ideal chain R_g's. This reveals that each of the polymers in the thinnest films is highly confined, with an overall thickness that is less than the unperturbed diameter (ca. one radius) of the macromolecule.

Figure 3 indicates a correlation between the magnitude of $\langle u^2 \rangle$ in the bulk and the degree to which there is a suppression of $\langle u^2 \rangle$ below the calorimetric glass transition. For example, PC has both the largest mean-square displacements and the strongest suppression of $\langle u^2 \rangle$. At the calorimetric T_g (425 K), the bulk $\langle u^2 \rangle$ value is 2.4 Å^2 in PC, but it is diminished to 0.7 Å^2 in the R_g-thick film. This corresponds to a reduction of 71%. For PMMA, the bulk $\langle u^2 \rangle$ at the calorimetric T_g (395 K) is smaller, 1.3 Å^2, with a decrease to 0.7 Å^2 in the R_g-thick film. This 46% reduction of $\langle u^2 \rangle$ is less dramatic in PMMA than in PC. In contrast, $\langle u^2 \rangle$ is exceedingly small in bulk PVC at T_g (358 K), being approximately 0.5 Å^2. Correspondingly, there is no reduction of $\langle u^2 \rangle$ in the R_g-thick PVC film.

The sizeable $\langle u^2 \rangle$ values in bulk PC are readily understood. PC is well known for its extensive segmental or local molecular mobility in the glassy state. The types of motions that occur in concert deep within the glassy state include librations and rotations of the isopropylidene methyls,[24–28] π flips of the phenyl rings,[26,29–32] and cis–trans isomerizations of the carbonate moieties.[24,33–36] The first two of these groups are hydrogenous and therefore dominate $\langle u^2 \rangle$ because of the large incoherent scattering cross section. For an appreciation of the sub-T_g contribution of the segmental methyl and phenyl ring motions to $\langle u^2 \rangle$, it is instructive to study deuterium-substituted PC. Replacing the methyl and phenyl hydrogens with deuterium atoms greatly reduces their elastic scattering cross section (now mostly coherent), thereby masking their contribution. The resulting $\langle u^2 \rangle$ values for the corresponding deuterated PC (bulk) in Figure 3 are significantly less than the hydrogenated analogues, especially below T_g. In the deuterated PC, $\langle u^2 \rangle$ evolves linearly (harmonically) with T and attains a value of just 0.5 Å^2 at the calorimetric glass transition. This is in stark contrast to hydrogenated PC, for which $\langle u^2 \rangle$ is 2.4 Å^2 at the same T.

The implication is that the large $\langle u^2 \rangle$ values in glassy PC films reflect segmental or localized motions, not Brownian motions of the main chain. Such diffusive motions, which give rise to viscous flow, do not occur until T_g is exceeded. By using *segmental*, we imply that the motion does not necessarily require significant excursions of the main chain. This is clear from the deuterated PC: once the highly mobile segmental motions are masked, $\langle u^2 \rangle$ only becomes appreciable above T_g. This is analogous to PVC, for which $\langle u^2 \rangle$ does not increase significantly until the rubbery state is entered. PVC is a linear chain lacking segmental or side group with extensive mobility, and this means that the dynamics of the hydrogen moieties directly reflect motions of the main chain; the hydrogen does not start moving significantly until the Brownian motions are enabled above T_g. This is also nominally consistent with the observation that industrial uses of PVC typically require small-molecule plasticizer additives or diluents to enhance the molecular mobility.[37]

These observations are intriguing because they point to the notion that highly dynamic glasses, having extensive segmental mobility below the calorimetric T_g, are more susceptible to confinement below the glass transition. That $\langle u^2 \rangle$ is severely curtailed in the thin PC films raises the question of how the fundamental properties of the glass change in the highly confined thin films. Other studies show that freezing these motions via synthetic routes, that is, imposing steric re-

strictions, transforms normally ductile and tough PC into a brittle plastic.[38,39] Is it conceivable that a similar effect is induced by the state of confinement in the thin films? It is further known that the onset of these phenyl ring flips and methyl rotations in bulk PC coincides[40,41] with the sub-T_g relaxation (we do not imply that these motions are necessarily the origin of this relaxation) near 175 K, which is commonly called the β or γ relaxation in dielectric or dynamic mechanical spectroscopy. This raises the intriguing question of whether the pronounced reduction of $\langle u^2 \rangle$ in the thin PC films points to a suppression of this characteristic sub-T_g relaxation and, therefore, a fundamental change in the nature of the glass. Likewise, it would be interesting to determine if the nature of the PVC glass is less affected by thin-film confinement. These considerations may become significant when polymers such as PC and PVC are fabricated into nanostructures (i.e., through nanoimprint lithography) for which the mechanical and physical properties of the glass are important.

The length scale cannot be ignored. The main graph of Figure 3(C) seems to suggest that glassy PVC is unaffected by thin-film confinement; the $\langle u^2 \rangle$ values are nearly identical below the calorimetric T_g for the bulk and 220-Å film. These data came from low-**Q** detectors, with which the longer length scale motions, more commensurate with localized segmental motions, were probed. However, a different conclusion can be obtained from the high-**Q** detectors, as shown in the inset of Figure 3(C). The high-**Q** data reflect more localized and faster motion (probably an extension of the harmonic oscillations that exist at 50 K) and clearly show suppression below T_g upon thin-film confinement. These observations are reasonable because PVC naturally lacks the segmental or side group motion (e.g., methyl rotations or phenyl ring flips) that would be probed by the low-**Q** detectors. We do not see a strong change in these low-**Q** data upon confinement because the relevant or, more appropriately, susceptible motions are lacking. However, at finer length scales, the effects of confinement are evidenced and are consistent with the reduced scattering intensities in Figure 1(C). This ability to probe the dynamics at different length scales with neutron scattering is a powerful tool for understanding glass dynamics.

It seems remarkable that the highly localized motions reflected in $\langle u^2 \rangle$ can be affected when the film thickness is still orders of magnitude greater than the amplitude of the motion. For example, intuition tells us macromolecular dimensions typically do not affect local or segmental motions, such as sub-T_g relaxations. However, if thin-film confinement alters the chain conformation, affecting in turn the nature of the intramolecular and intermolecular packing, then we could envisage changes in the highly local motions. A reduction of $\langle u^2 \rangle$ could be rationalized if molecules pack more tightly in the thin films, being more strongly caged by their neighboring segments. It remains to be seen how important R_g is with respect to the film thickness for observing these $\langle u^2 \rangle$ confinement effects. We have yet to study $\langle u^2 \rangle$ film thickness deviations for a broad range of molecular masses.

$\langle u^2 \rangle$ and the Apparent Glass Transition in Thin Polymer Films

Up to this point, we have not discussed how $\langle u^2 \rangle$ is related to T_g in thin polymer films. In a wide variety of glass-forming liquids, it is well documented that $\langle u^2 \rangle$ goes through a sharp increase at the calorimetrically defined T_g,[6,8,10,12,42,43] which is consistent with the sudden drop in η. Extending this phenomenology to thin films, Figure 3 seemingly indicates that thin-film confinement leads to an increase in the apparent T_g for all of these polymers. This conclusion, however, is not clear-cut when we consider complementary data obtained with other measurements. For example, X-ray reflectivity measurements of the thermal expansion in PC films indicate the opposite trend: T_g decreases for the 75-Å film.[3] To further clarify this situation, we compare X-ray reflectivity, beam positron annihilation lifetime spectroscopy (PALS), and incoherent neutron scattering measurements for an identical set of PC films.[44] Although the details of this study are not described here, both X-ray reflectivity and PALS suggest a decrease in the apparent T_g, whereas neutron scattering points to an increase. However, the thermal expansion coefficients from the X-ray reflectivity and PALS measurements display a pronounced decrease with the film thickness, which is consistent with the reduced amplitude of $\langle u^2 \rangle$. Optical[45,46] and thermal probe studies[47] of PMMA films on SiO_x and HMDS substrates also display opposite T_g shifts in comparison with the neutron scattering results. These studies report a T_g increase for the R_g-thick film on the SiO_x substrate but a T_g decrease on the HMDS surface. This is in contrast to the $\langle u^2 \rangle$ measurements on

the HMDS substrate, which does not immediately support a reduced T_g.

The reason that the T_g-like kink in $\langle u^2 \rangle$ does not track other traditional measures of T_g in thin films is poorly understood. This obviously raises fundamental questions about the nature of glass formation in thin polymer films. The glass transition is the onset of large-scale cooperative motions, and it seems that the length scale for these motions would be restricted by the thin-film confinement. It is also worth emphasizing that T_g shifts are normally inferred from changes in thermodynamic property measurements (specific heat, thermal expansion, etc.) performed under nonequilibrium conditions. A frequency or timescale is always implicit in these measurements, dependent on the rate at which the property is probed. It seems likely that the timescales over which a polymer equilibrates could be quite different in thin films (with respect to the bulk) and that these changes could be measurement-specific (dependant on the frequency scale of the measurement). It is well known from surface force apparatus measurements of confined liquid films (both polymer and small-molecule) that the viscoelastic timescales in bulk and molecularly confined films are generally not the same.[48–51] In this respect, it is unclear if the thin-film measurements are comparable to those of the bulk. Therefore, we must be careful when relating the kink in various thermodynamic properties as a function of temperature to the glass transition; the interpretation of these features must be reexamined on a property-by-property basis to determine if the resulting information predicts mobility changes in the thin polymer films. This notion will be developed in greater detail throughout this article.

It is interesting to examine the thermophysical behavior in the thinnest PC, PMMA, and PVC films. Figure 5 compares the mean-square displacement in all three of the polymers when they are confined to an R_g-thick film. The expanded vertical scale in comparison with Figure 3 reveals the thermal evolution of $\langle u^2 \rangle$ in greater detail. For each polymer, a set of two connected vertical arrows is superimposed on the graph. The leftmost arrow of the pair (which notably does not coincide with a kink in the curve) corresponds to the bulk calorimetric T_g. The rightmost arrow indicates the strong upturn in $\langle u^2 \rangle$, which, remarkably, occurs at $T = 1.2T_g$ in all of the polymers here. This crossover is provocative in connection with other phenomenology of glass-forming liquids that also

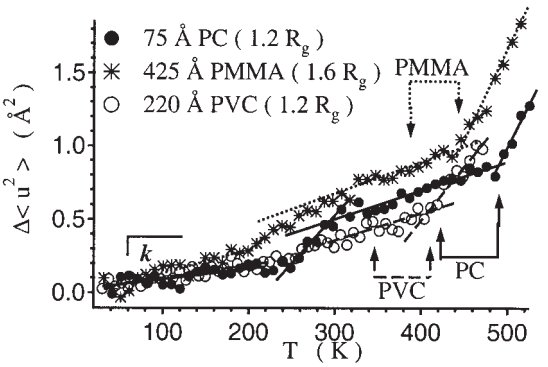

Figure 5. Comparison of PC, PMMA, and PVC films that are all approximately $1R_g$ thick. The expanded vertical scale (cf. Fig. 3) reveals greater detail in the thermal evolution of $\langle u^2 \rangle$. For each curve, there are two sets of vertical arrows. In each instance, the left arrow indicates the calorimetric T_g determined from the bulk material, whereas the right arrow corresponds to $1.2T_g$ and a strong increase in $\langle u^2 \rangle$ (the implications of this are discussed in the text). This plot also demonstrates the low-temperature linear regime (<200 K), in which κ is determined (see Fig. 6 and the discussion). The vertical error bars denote the standard uncertainties of $\langle u^2 \rangle$.

coincide with $T = 1.2T_g$ (in the so-called strong glasses, this crossover can be closer to $1.5T_g$). These changes include, but are not limited to, deviations from both the Stokes–Einstein (diffusion and η) and Debye–Einstein (reorientation time and η) relationships,[52–54] a bifurcation of the α- and β-relaxation processes,[52,55,56] the breaking of ergodicity as predicted by mode coupling theory,[57,58] and a crossover between the two Vogel–Fulcher relations commonly needed to fit relaxation data above T_g.[59–64] Clearly, there is a strong precedent for a characteristic glass-formation temperature near $1.2T_g$ to $1.5T_g$. The observation here that this crossover temperature is approximately $1.2T_g$ is also consistent with the fact that polymers are generally considered fragile glass formers. However, this does not explain why such a crossover would be exacerbated in the exceedingly thin films, whereas the conventional T_g is seemingly suppressed. At this point, we can only speculate on the origins of this effect.

Vibrational Stiffening or Caging in Thin Polymer Films

As discussed previously, the estimate of $\langle u^2 \rangle$ from eq 2 is based on a harmonic approximation, which is strictly violated by the high-temperature, non-

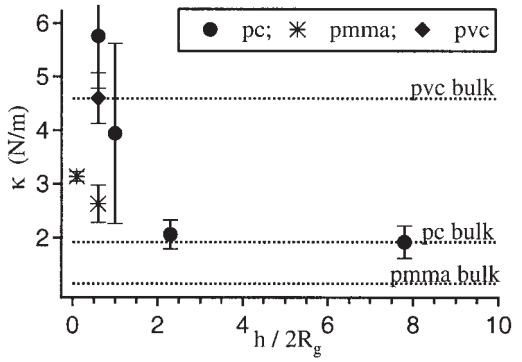

Figure 6. Variations in κ as a function of the normalized film thickness. The dashed lines indicate κ for the bulk material. PC exhibits strong vibrational stiffening with decreasing film thickness, whereas PVC remains bulklike even in the R_g-thick film. The vertical error bars indicate the standard uncertainties of κ.

linear regimes in Figures 3–5. However, below 200 K, the thermal evolution of $\langle u^2 \rangle$ is linear, and it is reasonable to assume that the atoms are trapped in local potential energy minima. In this regime, the equipartition theorem can be used to quantify the stiffness or resistance to displacement in terms of a harmonic force constant (or vibrational spring constant): $\kappa = 3k_BT/\langle u^2 \rangle$ (where k_B is the Boltzmann constant and T is the temperature). The low-temperature slope of $\langle u^2 \rangle$ versus T is inversely proportional to the elastic force constant (κ). In this picture, the confinement-induced suppression of $\langle u^2 \rangle$ corresponds to an increase in the vibrational stiffness, as summarized in Figure 6 as a function of h (normalized by $2R_g$, which is nominally the diameter of the macromolecule). For comparison, the dashed lines indicate κ for the bulk materials. In broad terms, κ ranges from 1 to 6 N/m in the polymer thin films. These values are comparable to analogous measurements of proteins below 200 K.[15] In contrast, κ for pure Si is 78.5 N/m[65] and one-to-two orders of magnitude greater than that of the polymer films. This agrees with the elastic modulus of Si, which is also one-to-two orders of magnitude greater than that of most polymers.

Figure 6 indicates that thin-film confinement significantly stiffens the local motions of PC, whereas virtually no changes can be observed for PVC. This is consistent with the earlier discussion of the extensive molecular mobility in glassy PC. Confinement curtails the longer range glassy motions, as indicated by the elastic stiffening, by which the predominantly localized motions of PVC remain unchanged. Of course, we must be cognizant of the nature of these motions. We have already discussed how phenyl ring and methyl group motions in PC are emphasized in the $\langle u^2 \rangle$. To this end, when these motions are constrained in the 75-Å PC film ($\kappa = 5.8 \pm 1.0$ N/m), it is notable and somewhat reassuring that that elastic stiffness becomes equivalent to that of bulk PVC ($\kappa = 4.6 \pm 0.5$ N/m), in which these motions are naturally absent and κ more so reflects interchain vibrations. As with the amplitudes of $\langle u^2 \rangle$, PC and PVC represent the extremes in terms of low-temperature vibrational stiffening. The R_g-thick PC, PMMA, and PVC films stiffen by approximately 200, 130, and 0%, respectively, in comparison with the bulk vibrations. In short, thin-film confinement increases the extent of intermolecular interactions in those glasses, which naturally possess extensive mobility. We develop this notion of caging in greater detail later.

Previously, we mentioned that in bulk glasses it is intriguing that $\langle u^2 \rangle$ and microscopic motions faster than a nanosecond correlate with the T_g from macroscopic variables, such as the enthalpy or specific volume, which are measured on a timescale of approximately seconds or minutes. However, this intriguing behavior can be understood if $\langle u^2 \rangle$ reflects the fast relaxations or rattling motions of an atom or molecule inside a cage of an unoccupied volume defined by its nearest neighbors. In the glass, this cage is rigid, but heating through the glass transition induces viscous flow and a sudden increase in the cage size that naturally leads to a simultaneous increase of $\langle u^2 \rangle$. Simulations[66,67] have revealed that the motions of a particle inside the cage (i.e., $\langle u^2 \rangle$) go through three distinct regimes as a function of time. At very short times t, extending to about a picosecond, the trajectories are ballistic ($\langle u^2 \rangle \sim t^2$). Intermediate times greater than a picosecond show that $\langle u^2 \rangle$ is time-invariant because of the caging effect; $\langle u^2 \rangle$ cannot exceed the dimensions of the cage. The time-invariant plateau of $\langle u^2 \rangle$ extends for many orders of magnitude until the cage disintegrates through diffusive motions of the neighbors, that is, the glass transition. These diffusive motions ($\langle u^2 \rangle \sim t$) would be consistent with the conventional timescale of tens of seconds associated with the glass transition. To understand the relation of $\langle u^2 \rangle$ with the glass transition, we should appreciate the time invariance of the cage size or $\langle u^2 \rangle$. The nanosecond time resolution of the HFBS spectrometer is well beyond the ballistic limit, and this means that $\langle u^2 \rangle$ reflects the mo-

tions confined by the glassy intermolecular cage. The time invariance means that the amplitude of $\langle u^2 \rangle$ is the same averaged over either nanoseconds or seconds, as long as the materials are below T_g. Within this context, it may be easier to reconcile the relation of $\langle u^2 \rangle$ with the traditional lower frequency estimates of T_g.

The interpretation of $\langle u^2 \rangle$ in terms of intermolecular caging is supported by recent PALS measurements of glassy glycerol, propylene glycol, propylene carbonate, and orthoterphenyl.[43] PALS quantifies the nanometer-sized density heterogeneities in glassy hydrocarbon materials, being an effective way of directly measuring the unoccupied volume available for intermolecular rattling motions. Glycerol and propylene glycol displayed smaller values of $\langle u^2 \rangle$ below T_g and noticeably stiffer κ values than orthoterphenyl and propylene carbonate. This suggested stronger intermolecular caging in glycerol and propylene glycol, which was borne out by the PALS measurements; their glassy structures were also significantly less open and possessed larger regions of unoccupied volume.

It appears that caging and the concomitant reduction of mobility or $\langle u^2 \rangle$ are geometric aspects of confinement, independent of the interactions with the confining surface. This is supported by the fact that $\langle u^2 \rangle$ is equally suppressed in thin PMMA films supported on native oxide (favorable) and HMDS (unfavorable) substrates. Although this may seem to contradict the optical[45,46] and thermal probe[47] measurements, the trend is consistent with surface force measurements of the shear viscosity in exceedingly thin liquid films. These measurements suggest that the confinement induces more efficient intermolecular packing when the film thickness approaches nominally 10 times the molecular diameter (ca. 100–200 Å in most polymers). This leads to an increase in the shear viscosity and the elastic properties of the film, regardless of the interactions between the confining mica rods of the surface force apparatus and the liquid.[48–51] These observations are phenomenologically relevant, given correlations between $\langle u^2 \rangle$ and η;[68,69] that is, η has been observed to increase exponentially with $1/\langle u^2 \rangle$ in bulk glasses (as discussed later). In this respect, the reduction of $\langle u^2 \rangle$ with decreasing film thickness points to an increase in η.

Taken together, the neutron scattering and surface force measurements thus far suggest that the mobility or amplitude of the thermal motion is reduced in thin, supported polymer films. These changes in the mobility do not coincide with the thermodynamic estimates of the glass transition made under quasiequilibrium conditions. A large number of studies have focused on T_g shifts of this kind as an indicator of changes in the thin-film mobility, and this interpretation should be considered with caution. For example, we previously used the example of PC, for which the apparent T_g kink from specular X-ray reflectivity[3] and PALS[44] shifted to lower T with decreasing film thickness, potentially indicating an increase in the mobility. However, $\langle u^2 \rangle$ showed a clear reduction of magnitude with decreasing film thickness, and this was also consistent with the reduced thermal expansion coefficients from reflectivity and PALS. Now if (hypothetically) PC were a technologically relevant photoresist film, the apparent T_g decrease from thermal expansion and/or PALS data might lead to predictions that the kinetics of photoacid transport would be enhanced in the thin films. However, if the overall mobility is reduced, the shift in the relative position of the T_g kink may be irrelevant, and ultimately the kinetics could be hindered with respect to very thick films. This is illustrated in greater detail later.

$\langle u^2 \rangle$ and Transport in Thin Polymer Films

In the previous discussion, we have shown how local segmental motions deep in the glassy state lead to an increase of $\langle u^2 \rangle$. It is also well understood that segmental molecular motions, either along the backbone or localized to side groups, dramatically affect the kinetics of small-molecule transport through polymeric materials.[70,71] Several authors have argued that these motions produce a gating effect that regulates gas or small-molecule transport through the interchain regions of amorphous polymers.[72–75] This effect should be of consequence in deep UV lithography, in which a photochemically generated acidic proton (H^+) must diffuse through a photoresist film, accompanied by some sort of counterion, to induce multiple chemical reactions. Likewise, aqueous-based developers are used to dissolve photoresist films, and this means that H_2O diffusion into the photoresist film is also important. With an approximate diameter of 3 Å for H_2O, these species should readily diffuse through the amorphous regions of a polymer for which the interchain distances (between atom centers) are approximately 5 Å. However, it remains to be seen if the high-frequency local chain motions reflected in $\langle u^2 \rangle$,

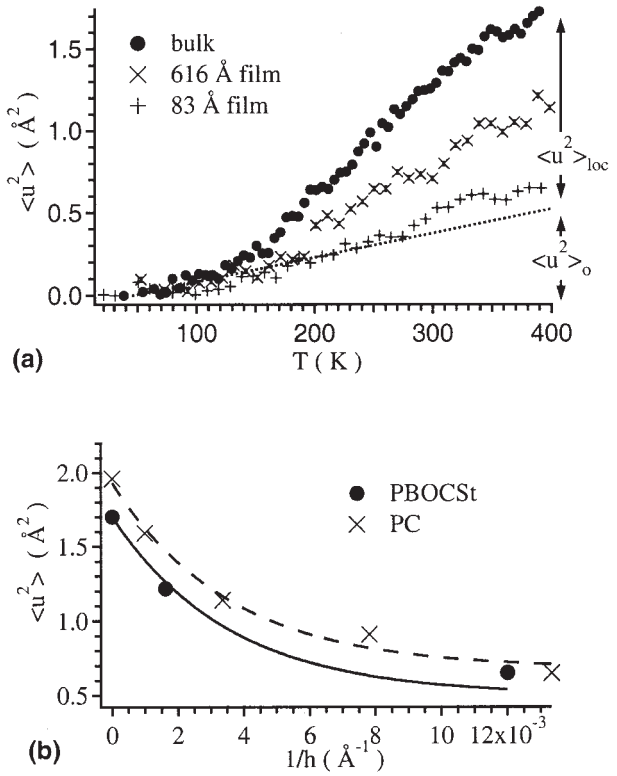

Figure 7. (a) Thermal evolution of $\langle u^2 \rangle$ in PBOCSt as a function of h below the thermal decomposition temperature. A linear fit (dashed line) of the bulk data between 40 and 80 K has been used to extrapolate an approximation for the harmonic-like vibrational contributions ($\langle u^2 \rangle_0$) at elevated temperatures. The difference between $\langle u^2 \rangle$ and $\langle u^2 \rangle_0$ is defined as $\langle u^2 \rangle_{loc}$, in the spirit of Buchenau and Zorn[68] and Kanaya et al.[69] (b) $\langle u^2 \rangle$ data as a function of $1/h$ fit to a function form of $\langle u^2 \rangle = A \exp(B/h)$ for both PBOCSt from part a and PC films from Figure 3(A). The solid and dotted lines indicate the fits for PBOCSt and PC, respectively. The standard uncertainty of $\langle u^2 \rangle$ is typically less than the size of the data marker.

and their corresponding changes with the film thickness, affect H^+ reaction–diffusion kinetics or H_2O mobility in these interchain regions. Given the amplitude and timescale of $\langle u^2 \rangle$, it seems reasonable to anticipate that these dynamics would be germane to the transport of H^+, H_2O, or other small-molecule species.

Figure 7(a) displays the $\langle u^2 \rangle$ values as a function of h for PBOCSt, one of the most common photoresist materials for 248-nm-deep UV lithography. Like PC, bulk PBOCSt has extensive local mobility in the glass state, as evidence by the large values of $\langle u^2 \rangle$ below T_g (T_g has been estimated to be 430 K). The data in Figure 7(a) do not extend to higher T to reveal the anticipated kink in $\langle u^2 \rangle$ because PBOCSt goes through a thermal decomposition reaction close to T_g. The effects of this decomposition reaction on $\langle u^2 \rangle$ have been described elsewhere in detail.[4] Nevertheless, it is evident that increasing the degree of thin-film confinement below T_g decreases the amplitude of $\langle u^2 \rangle$. We then anticipate a concomitant reduction in the transport properties through confined PBOCSt films.

The H^+ mobility in thin PBOCSt films has been measured directly with model bilayer diffusion couple experiments described elsewhere.[76] In brief, a thick film of fully deprotected PBOCSt (called PHOSt) containing photoacid generator (PAG) molecules is spin-cast over the top of a thin, PAG-free film of PBOCSt. When the bilayer structure is exposed to UV radiation and heated, H^+ produced in the top PHOSt layer diffuses into the PBOCSt underlayer and induces the deprotection. By measuring how far the H^+ reaction front propagates into the PBOCSt underlayer as a function of the bake time, we can extract an effective reaction front diffusion coefficient (D_{eff}). Figure 8 shows that D_{eff} at 383 K decreases approximately in an exponential manner when h of the PBOCSt underlayer is diminished. Qualitatively, this is consistent with the notion that a reduced $\langle u^2 \rangle$ value leads to hindered diffusivity. In the following, we make this correlation more quantitative.

Correlations between $\langle u^2 \rangle$ and PALS[43,77–79] are used to develop the argument that $\langle u^2 \rangle$ also reflects the openness of a material structure. This is also consistent with the observation in Se that for a given temperature, $\langle u^2 \rangle$ is noticeably smaller in

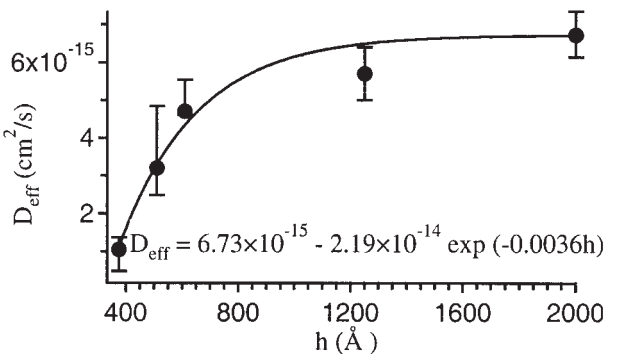

Figure 8. D_{eff} (and standard uncertainties), as reported elsewhere,[76] as a function of h. The solid line indicates an exponential fit function forced to plateau at the D_{eff} value of the thickest film.

the crystalline state than in the less dense glass, in which the heterogeneity and lower packing density enable larger $\langle u^2 \rangle$ values.[68] However, the precise relation between $\langle u^2 \rangle$ and the average unoccupied or cavity volume (as evidenced by positron annihilation), sometimes loosely (and often incorrectly) called the free volume (V_f), has not been established. Classical models of mobility suggest that the dynamic properties of a glass strongly decrease as V_f approaches a limiting low-temperature value, $V_f(T \rightarrow 0) = V_{f,0}$. Likewise, Doolittle[80] suggested that η varies as $\eta = \eta_0 \exp[-\gamma V_{f,0}/(V_f - V_{f,0})]$ (where γ is an adjustable parameter and η_0 is the pre-exponential constant), with a similar form rationalized theoretically by Cohen and Turnbull.[81] Although in the Doolittle arguments V_f is related directly to the specific volume, it is not unreasonable to anticipate correlations of this quantity with the unoccupied microscopic volume reflected in $\langle u^2 \rangle^{3/2}$.[82] In terms of H^+ or H_2O mobility, it seems reasonable to anticipate that larger $\langle u^2 \rangle^{3/2}$ volumes would lead to enhanced diffusion.

Recent Lennard–Jones bead–spring simulations of polymer fluids by Starr et al.[82] have been used to consider these relations precisely. In particular, they show a strong correlation between $\langle u^2 \rangle^{3/2}$ and a well-defined type of free volume. Specifically, $\langle u^2 \rangle^{3/2}$ corresponds to the mean volume within which the center of an atom (bead) can rattle when the surrounding particles are fixed, and this definition has a rigorous relation to the equation of state for hard-sphere fluids.[83–85] Likewise, Buchenau and Zorn[68] empirically demonstrated that η of liquid and glassy Se exponentially scales with $1/\langle u^2 \rangle$:

$$\eta = \eta_0 \exp(\langle u^2 \rangle_0 / \langle u^2 \rangle_{loc}) \tag{3}$$

where $\langle u^2 \rangle_0$ is a constant and $\langle u^2 \rangle_{loc}$ is defined as the difference in $\langle u^2 \rangle$ between the crystalline and liquid–glassy states. Kanaya et al.[69] showed that eq 3 can also be successfully applied to liquid and glassy polybutadiene. Starr et al.[82] also found a relation in the form of eq 3 in their model glass-forming liquid, and there are comparable theoretical predictions in support of the notion that a large $\langle u^2 \rangle$ value should lead to enhanced transport.[86–88]

If we assume that $\langle u^2 \rangle$ influences the mobility of H^+ in a PBOCSt film, then eq 3 suggests that the decrease of $\langle u^2 \rangle$ with the film thickness corresponds to a decrease in the H^+ diffusion coefficient (assuming an Einstein-like dependence: $\eta \approx kT/aD$). This can be used to estimate the relative change of η or the diffusion coefficient due to confinement if we assume that $\langle u^2 \rangle_0$ does not change with the film thickness:

$$\frac{\eta_{film}}{\eta_{bulk}} = \frac{D_{bulk}}{D_{film}} = \exp\left(\frac{\langle u^2 \rangle_0}{\langle u^2 \rangle_{loc,film}} - \frac{\langle u^2 \rangle_0}{\langle u^2 \rangle_{loc,bulk}} \right) \tag{4}$$

where η_{film} and η_{bulk} are the film viscosity and bulk viscosity, respectively, and D_{film} and D_{bulk} are the film diffusion coefficient and bulk diffusion coefficient, respectively. Unfortunately, PBOCSt does not crystallize like Se, and $\langle u^2 \rangle_{loc}$ cannot be directly measured. However, it is equally reasonable to estimate the level of these harmonic contributions that do not give rise to diffusion through the fitting of the bulk $\langle u^2 \rangle$ data between 40 and 80 K to a linear function and through extrapolation to a high temperature. $\langle u^2 \rangle_{loc}$ can be approximated as the difference between $\langle u^2 \rangle$ at any temperature and the linear extrapolation from the low-temperature harmonic behavior. Figure 7(a) demonstrates this approximation for the PBOCSt films.

From the estimates of $\langle u^2 \rangle_0$ and $\langle u^2 \rangle_{loc}$, eq 4 can be used to predict the corresponding decrease in the effective H^+ reaction-diffusion coefficient for the thin films. At 383 K (the same temperature used for the bilayer experiments in Fig. 8) Figure 7(a) reveals that $\langle u^2 \rangle_0$ is 0.50 Å^2, whereas the $\langle u^2 \rangle$ values in the bulk PBOCSt, the 616-Å film, and the 83-Å film are 1.70, 1.22, and 0.65 Å^2, respectively. From these values, we can calculate $\langle u^2 \rangle_{loc}$ and predict the D_{bulk}/D_{film} ratio as a function of the film thickness, as shown by the two asterisk data markers in Figure 9. It would be helpful if more $\langle u^2 \rangle$ data existed to define the thickness dependence of D_{bulk}/D_{film} in more detail, but the qualitative trend seems clear. In lieu of obtaining more data, we note that for PC (for which more films were available), the thickness dependence of $\langle u^2 \rangle$ was reasonably approximated by $\langle u^2 \rangle = A \exp(B/h)$, where A and B are system-dependent constants. This is shown in Figure 7(b), which shows the $\langle u^2 \rangle$ data at 383 K as a function of the inverse film thickness for both PC and PBOCSt. The dashed and solid lines indicate fits to the aforementioned exponential for PC and PBOCSt, respectively; the exponential expression captures the spirit of the thickness variation of $\langle u^2 \rangle$, even if there are limited PBOCSt data. For the PBOCSt fit, the prefactors A and B are chosen so that the

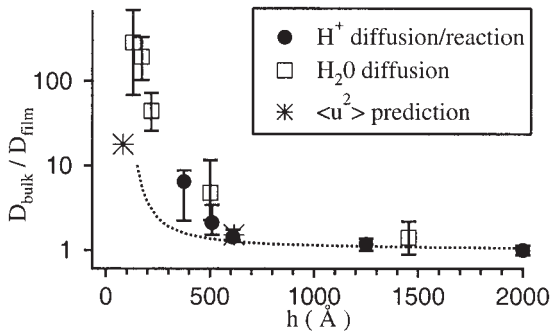

Figure 9. D_{bulk}/D_{film} as a function of h. The circles represent the D_{eff} values presented in Figure 8. The asterisks and dashed line represent ratios predicted from $\langle u^2 \rangle$ and eq 4 and the exponential fit to the PBOCSt data in Figure 7(b), respectively. The open squares represent the apparent H_2O diffusion coefficient reported elsewhere.[89] All three techniques show reduced mobility at a similar thin-film confinement length scale. The standard uncertainties associated with each measurement either are indicated by the error bars or are less than the size of the data marker.

appropriate boundary conditions are met: $\langle u^2 \rangle = 1.70$ Å^2 at $1/h = 0$ and $\langle u^2 \rangle = 0.50$ Å$^2 = \langle u^2 \rangle_0$ at $1/h = \infty$. This ensures that the fit reaches the proper bulk value in an infinitely thick film and that it does not drop below what we have estimated to be the lower harmonic limit in Figure 7(a). The dotted line in Figure 9 indicates the D_{bulk}/D_{film} ratio obtained from the exponential fit in Figure 7(b).

Figure 9 also displays the D_{bulk}/D_{film} ratios obtained from the D_{eff} and bilayer diffusion couple experiments. In this case, D_{bulk} is taken to be the D_{eff} value for the thickest film, the value of the exponential plateau in Figure 8. The agreement between the D_{bulk}/D_{film} data sets from the $\langle u^2 \rangle$ and D_{eff} data is quite reasonable, and this suggests that the reduction of $\langle u^2 \rangle$ in the thin film is linked to the suppression of the reaction front propagation kinetics. This suggests that our simplistic model may be pointing to the correct underlying physics for the retardation of the reaction front in exceedingly thin PBOCSt films.

We further generalize the notion of reduced transport in the thin PBOCSt films through H_2O diffusion experiments. The bilayer experiments are complicated by the fact that D_{eff} reflects both H^+ diffusion (which, although ignored here, would seemingly require complementary counterion diffusion) and reaction. It is difficult to determine if the reduction of D_{eff} with the film thickness is due to changes in the diffusivity or reactivity. In comparison, H_2O transport measurements simplify the situation because water does not react with PBOCSt. A series of quartz crystal microbalance (QCM) studies, described in detail elsewhere,[89] have been used to study H_2O diffusion into dry PBOCSt as a function of the film thickness. PBOCSt films were spin-cast onto the QCM substrate, dried in a vacuum oven, and then exposed to 100% relative humidity inside the QCM. From the shift in the frequency, the mass of the H_2O uptake could be monitored as a function of time. Figure 9 displays the D_{bulk}/D_{film} ratio obtained from these H_2O absorption measurements.

It is striking that all three D_{bulk}/D_{film} data sets (from $\langle u^2 \rangle$, D_{eff}, and H_2O diffusion) nominally show the same deviations with the film thickness. We do not necessarily interpret this as evidence that the critical length scales for each of the three techniques are the same. Instead, this strongly suggests that the reduced amplitude of the thermal motions with decreasing film thickness, evidenced by the reduction of $\langle u^2 \rangle$, is a general phenomenon impacting a wide range of diffusion and transport properties in these thin films. This is analogous to the discussion of how $\langle u^2 \rangle$ correlates with macroscopic variables such as η and T_g. More importantly, because all the polymer films studied here (not just PBOCSt) demonstrate some form of reduced $\langle u^2 \rangle$ with decreasing film thickness, we might anticipate similar reductions of mobility, transport, and/or diffusion for the thin-film geometry. Preliminary H_2O diffusion measurements of single thick and thin films indicate that this is at least true for PC. We contrast these finding in light of the reduced molecular mobility with X-ray reflectivity measurements, which indicate that the apparent T_g of PC decreases with the film thickness.[3] Clearly, T_g estimates based on a kink in the thermal expansion are unreliable indicators of the changes in the molecular mobility in these thin films. On the other hand, $\langle u^2 \rangle$ seems to provide a good indication of the observed changes in the molecular mobility.

A large body of evidence is presented here supporting the notion that $\langle u^2 \rangle$ is predictive of changes in the dynamics at much larger time and spatial scales and that $\langle u^2 \rangle$ generally becomes reduced as the thickness of the polymer film decreases. This discussion began with a consideration of the relation between η and $\langle u^2 \rangle$ (i.e., eq 3). The established phenomenology, which seems to extend to films, implies that $1/\langle u^2 \rangle$ is proportional to ln η. This motivates the presentation of the $\langle u^2 \rangle$

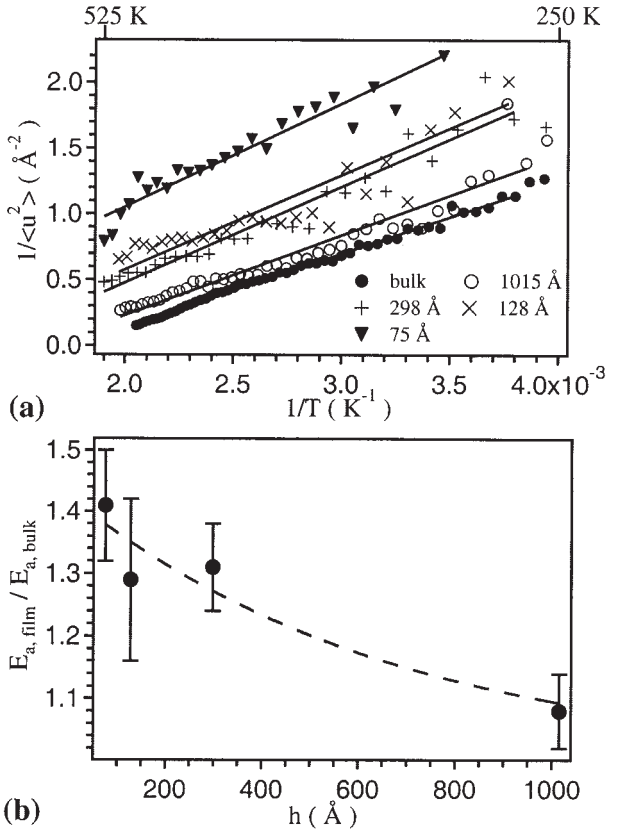

Figure 10. (a) $\langle u^2 \rangle$ data (from eq 3) presented in an Arrhenius format for the PC films described in Figure 3(a). The slope of the linear fits defines an apparent E_a that is plotted as a function of h in part b. (b) Exponential fit (shown as a dashed line intended to guide the eye) forced to converge at a ratio of unity for an infinitely thick film. The standard uncertainty of $\langle u^2 \rangle$ is comparable to the size of the data markers, whereas the standard uncertainties of the linear fits (and thus the E_a values) are indicated.

data in an Arrhenius format of $1/\langle u^2 \rangle$ versus $1/T$, as shown in Figure 10(a) for the PC films originally presented in Figure 3(A). The linearization of the $\langle u^2 \rangle$ data with this procedure seems remarkably good over a wide T range, with the slope proportional to the activation energy (E_a). Figure 10(b) displays the ratio of the film to bulk E_a's as a function of the film thickness. There is an appreciable increase in the apparent E_a with increasing film thinness; the effect is as large as 40% for the 75-Å films. The fit (dashed line) indicates that the data are consistent with an exponential decrease of $E_{a,film}/E_{a,bulk}$ with increasing film thickness, approaching 1.0 for an infinitely thick film. The increasing apparent E_a values support the notion that diffusive processes are made difficult by thin-film confinement. This presentation, though somewhat similar to the κ analysis in Figure 6, provides another way of quantifying the mobility changes in thin films. However, unlike Figure 6, the linearization in Figure 10(a) extends over a broad T range, extending from far below T_g to well above T_g, raising interesting questions about the determination of T_g from an apparent deviation from linearity in plots (e.g., Fig. 3). The increased E_a values are also consistent with the low-T vibrational stiffening data in Figure 6 and the ensuing discussion of enhanced caging. If the caging is strengthened by thin-film confinement, then larger E_a values are required to break up the cages and induce viscous flow, as indicated by Figure 10.

CONCLUSIONS

We have demonstrated how incoherent elastic neutron scattering measurements can be used to probe the dynamics in polymer films as thin as approximately 75 Å. The dynamics at a frequency of 200 MHz and faster are characterized in terms of $\langle u^2 \rangle$. After examining a broad range of polymers, we have generally found that $\langle u^2 \rangle$ is strongly reduced as the film thickness decreases, with little dependence on the specific polymer or substrate interactions above the calorimetric T_g. Below T_g, a decrease in $\langle u^2 \rangle$ with decreasing film thickness only occurs in those polymer that have extensive segmental or local molecular mobility in the glassy state; glassy polymers that lack local or segmental motion, instead being dominated by main-chain motions, show almost no change in $\langle u^2 \rangle$ upon confinement. We have further shown how the reduction of $\langle u^2 \rangle$ reflects other direct indications of reduced mobility in thin films, such as photoacid and water transport. Together, these findings present a general and strong indication of reduced mobility in thin polymer films and show that $\langle u^2 \rangle$ provides a useful tool for estimating the extent of this mobility. This differs from mobility estimates based on T_g's derived from thermodynamic parameters. Although such T_g estimates contain thermodynamically meaningful information, they are unreliable for predicting mobility changes with confinement.

This work is based on activities supported by the National Science Foundation (DMR-0086210) and the Defense Advanced Research Program Agency (DARPA)

Advanced Lithography Program (N66001-00-C-8803). The authors further acknowledge Marcus T. Cicerone and Francis W. Starr for their critical reviews of the manuscript.

REFERENCES AND NOTES

1. Karim, A.; Kumar, S. Polymer Surfaces, Interfaces, and Thin Films; World Scientific: Singapore, 1999.
2. Jones, R. A. L. Curr Opin Colloid Interface Sci 1999, 4, 153.
3. Soles, C. L.; Douglas, J. F.; Wu, W.-L.; Dimeo, R. M. Phys Rev Lett 2002, 88, 037401.
4. Soles, C. L.; Douglas, J. F.; Lin, E. K.; Lenhart, J. L.; Jones, R. L.; Wu, W.-L.; Goldfarb, D. L.; Angelopoulos, M. J Appl Phys 2003, 93, 1978.
5. Soles, C. L.; Douglas, J. F.; Wu, W.-L.; Dimeo, R. M. Macromolecules 2003, 36, 373.
6. Frick, B. Prog Colloid Polym Sci 1989, 80, 164.
7. Frick, B.; Fetters, L. J. Macromolecules 1997, 27, 974.
8. Frick, B.; Richter, D. Science 1995, 267, 1939.
9. Colmenero, J.; Arbe, A. Phys Rev B 1998, 57, 13508.
10. Angell, C. A.; Ngai, K. L.; McKenna, G. B.; McMillan, P. F.; Martin, S. W. J Appl Phys 2000, 88, 3113.
11. Doster, W.; Cusack, S.; Petry, W. Nature 1989, 337, 754.
12. Angell, C. A. Science 1995, 267, 1924.
13. Lehnert, U.; Réat, V.; Weik, M.; Zaccaï, G.; Pfister, C. Biophys J 1998, 75, 1945.
14. Deriu, A. Neutron News 2000, 11, 26.
15. Zaccaï, G. Science 2000, 288, 1604.
16. Certain commercial equipment and materials are identified in this article to specify adequately the experimental procedure. In no case does such identification imply recommendation by the National Institute of Standards and Technology, nor does it imply that the material or equipment identified is necessarily the best available for this purpose.
17. Frechet, J. M.; Eichler, E.; Ito, H.; Willson, C. G. Polymer 1983, 24, 995.
18. Lin, E. K.; Soles, C. L.; Goldfarb, D. L.; Trinque, B. C.; Burns, S. D.; Jones, R. L.; Lenhart, J. L.; Angelopoulos, M.; Willson, C. G.; Satija, S. K.; Wu, W.-L. Science 2002, 297, 372.
19. Gehring, P. M.; Neumann, D. A. Phys B 1998, 241, 64.
20. Settles, M.; Doster, W. Faraday Discuss 1996, 103, 269.
21. Prevorsek, D. C.; DeBona, B. T. J Macromol Sci Phys 1986, 25, 515.
22. Chinai, S. N.; Guzzi, R. A. J Polym Sci 1959, 41, 475.
23. Sato, M.; Koshiishi, Y.; Asahina, M. Polym Lett 1963, 1, 233.
24. Garfield, L. J. J Polym Sci Part C: Polym Symp 1970, 30, 551.
25. Spiess, H. W. Colloid Polym Sci 1983, 261, 193.
26. Schaefer, J.; Stejskal, E. O.; McKay, R. A.; Dixon, W. T. Macromolecules 1984, 17, 1479.
27. Schmidt, C.; Kuhn, K. J.; Spiess, H. W. Prog Colloid Polym Sci 1985, 71, 71.
28. Smith, P. B.; Brubeck, R. A.; Bales, S. E. Macromolecules 1988, 21, 2058.
29. Steger, T. R.; Schaefer, J.; Stejskal, E. O.; Mckay, R. A. Macromolecules 1980, 13, 1127.
30. Jones, A. A.; O'Gara, J. F.; Inglefield, P. T.; Bendler, J. T.; Yee, A. F.; Ngai, K. L. Macromolecules 1983, 16, 658.
31. Roy, A. K.; Jones, A. A.; Inglefield, P. T. Macromolecules 1986, 19, 1356.
32. Wehrle, M.; Hellmann, G. P.; Spiess, H. W. Colloid Polym Sci 1987, 265, 815.
33. Reading, F. P.; Faucher, J. A; Whitman, R. D. J Polym Sci 1961, 54, 556.
34. Matsuoka, S.; Ishida, Y. J Polym Sci Part C: Polym Symp 1966, 14, 247.
35. Stefan, D.; Williams, H. L. J Appl Polym Sci 1974, 18, 1279.
36. Watts, D. C.; Perry, E. P. Polymer 1978, 19, 248.
37. McCrum, N. G.; Read, B. E.; Williams, G. Anelastic and Dielectric Effects in Polymeric Solids; Wiley: London, 1967.
38. Liu, J.; Yee, A. F. Macromolecules 1998, 31, 7865.
39. Wu, J.; Xiao, C.; Klug, C. A.; Schaefer, J. J Polym Sci Part B: Polym Phys 2001, 39, 1730.
40. Davenport, W. A.; Manuel, A. J. Polymer 1977, 18, 557.
41. Schaefer, J.; Stejskal, F. O.; Buchdahl, R. Macromolecules 1977, 10, 384.
42. Frick, B.; Richter, D.; Petry, W.; Buchenau, U. Z Phys B: Condensed Matter 1988, 70, 73.
43. Ngai, K. L.; Bao, L.-R.; Yee, A. F.; Soles, C. L. Phys Rev Lett 2001, 87, 5901.
44. (a) Soles, C. L.; Douglas, J. F.; Wu, W.-L.; Peng, H.; Gidley, D. W. Mater Res Soc Proc 2002, 710, DD 3.7.1; (b) Soles, C. L.; Douglas, J. F.; Wu, W.-L.; Peng, H.; Gidley, D. W. Macromolecules 2004, 37, 2890.
45. Keddie, J. L.; Jones, R. A. L.; Cory, R. A. Faraday Discuss 1994, 98, 1.
46. Prucker, O.; Christian, S.; Bock, H.; Ruhe, J.; Frank, C. W.; Knoll, W. Macromol Chem Phys 1998, 199, 1435.
47. Fryer, D. S.; Nealy, P. F.; de Pablo, J. J. Macromolecules 2000, 33, 6439.
48. Horn, R. G.; Israelachvili, J. N. Macromolecules 1988, 21, 2836.
49. Granick, S. Science 1991, 253, 1374.
50. Hu, H.-W.; Granick, S. Science 1992, 258, 1339.
51. Levent Demirel, A.; Granick, S. Phys Rev Lett 1996, 77, 2261.
52. Rossler, E. Phys Rev Lett 1990, 65, 1595.

53. Fujara, F.; Geil, B.; Sillescu, H.; Fleischer, G. Z. Phys B 1992, 88, 195.
54. Chang, I.; Fujara, F.; Heuberger, B. G. G.; Mangel, T.; Sillescu, H. J Non-Cryst Solids 1994, 172, 248.
55. Hansen, C.; Stickel, F.; Berger, T.; Richert, R.; Fischer, E. W. J Chem Phys 1997, 107, 1086.
56. Hansen, C.; Stickel, F.; Richert, R.; Fischer, E. W. J Chem Phys 1998, 108, 6408.
57. Gotze, W.; Sjogren, L. Rep Prog Phys 1992, 55, 241.
58. Gotze, W. J Phys: Condens Matter A 1991, 11, 1.
59. Plazek, D. J.; Magill, J. H. J Chem Phys 1966, 45, 3038.
60. Greet, R. J.; Magill, J. H. J Phys Chem 1967, 71, 1746.
61. Plazek, D. J.; Magill, J. H. J Chem Phys 1968, 49, 3678.
62. Stickel, F.; Fischer, E. W.; Richert, R. J Chem Phys 1995, 102, 6251.
63. Stickel, F.; Fischer, E. W.; Richert, R. J Chem Phys 1996, 104, 2043.
64. Ngai, K. L.; Magill, J.; Plazek, D. J Chem Phys 2000, 112, 1887.
65. Flensburg, C.; Stewart, R. F. Phys Rev B 1999, 60, 284.
66. Donati, C.; Glotzer, S. C.; Poole, P. H.; Kob, W.; Plimpton, S. J. Phys Rev E 1999, 60, 3107.
67. Allegrini, P.; Douglas, J. F.; Glotzer, S. C. Phys Rev E 1999, 60, 5714.
68. Buchenau, U.; Zorn, R. Europhysics Letters 1992, 18, 523.
69. Kanaya, T.; Tsukushi, T.; Kaji, K.; Bartos, J.; Kristiak, J. Phys Rev E 1992, 60, 1906.
70. Crank, J.; Park, G. S. Diffusion in Polymers; Academic: London, 1968.
71. Neogi, P. Diffusion in Polymers; Marcel Dekker: New York, 1996.
72. Stuk, L. G. F. J Polym Sci Part B: Polym Phys 1990, 28, 127.
73. Haag, M.-B.; Koros, W. J.; Schmidhauser, J. C. J Polym Sci Part B: Polym Phys 1994, 32, 1625.
74. Ponitsch, M.; Gotthardt, P.; Gruger, A.; Brion, H. G.; Kirchheim, R. J Polym Sci Part B: Polym Phys 1997, 35, 2397.
75. Soles, C. L.; Yee, A. F. J Polym Sci Part B: Polym Phys 2000, 38, 792.
76. Goldfarb, D. L.; Angelopoulos, M.; Lin, E. K.; Jones, R. L.; Soles, C. L.; Lenhart, J. L.; Wu, W.-L. J Vac Sci Technol B 2001, 19, 2699.
77. Novikov, V. N.; Sokolov, A. P.; Strube, B.; Surovstev, N. V.; Duval, E.; Mermet, A. J Chem Phys 1997, 107, 1057.
78. Bartos, J.; Bandzuch, P.; Sausa, O.; Kristiakova, K.; Kristiak, J.; Kanaya, T.; Jenninger, W. Macromolecules 1997, 30, 6906.
79. Kanaya, T.; Tsukushi, T.; Kaji, K.; Bartos, J.; Kristiak, J. Phys Rev E 1999, 60, 1906.
80. Doolittle, A. K. J Appl Polym Sci 1951, 22, 1471.
81. Cohen, M. H.; Turnbull, D. J Chem Phys 1959, 31, 1164.
82. Starr, F. W.; Sastry, S.; Douglas, J. F.; Glotzer, S. C. Phys Rev Lett 2002, 89, 125501.
83. Hoover, W. G.; Ashurst, W. T.; Grover, R. J Chem Phys 1972, 57, 1259.
84. (a) Speedy, R. J. J Chem Soc Faraday Trans 2 1977, 73, 714; (b) Speedy, R. J. J Chem Soc Faraday Trans 2 1980, 75, 1643; (c) Speedy, R. J. J Chem Soc Faraday Trans 1980, 276, 693; (d) Speedy, R. J. J Chem Soc Faraday Trans 2 1981, 77, 329.
85. (a) Reiss, H.; Dell Hammerich, A. J Phys Chem 1986, 90, 6252; (b) Speedy, R. J.; Reiss, H. Mol Phys 1991, 72, 999; (c) Speedy, R. J.; Reiss, H. Mol Phys 1991, 72, 1015.
86. Hall, R. W.; Wolynes, P. G. J Chem Phys 1987, 86, 2943.
87. Dyre, J. C.; Olsen, N. B.; Christensen, T. Phys Rev B 1996, 53, 2171.
88. Zurcher, U.; Keyes, T. Phys Rev E 1999, 60, 2065.
89. Soles, C. L.; Jones, R. L.; Lenhart, J. L.; Prabhu, V. M.; Wu, W.-L.; Lin, E. K.; Goldfarb, D. L.; Angelopoulos, M. Proc SPIE 2003, 5039, 366.